Cell Reports
Physical Science

Article

DPP-based terpolymers for enhanced electrical stretchability via backbone engineering toward delocalized frontier molecular orbital

Graphical abstract

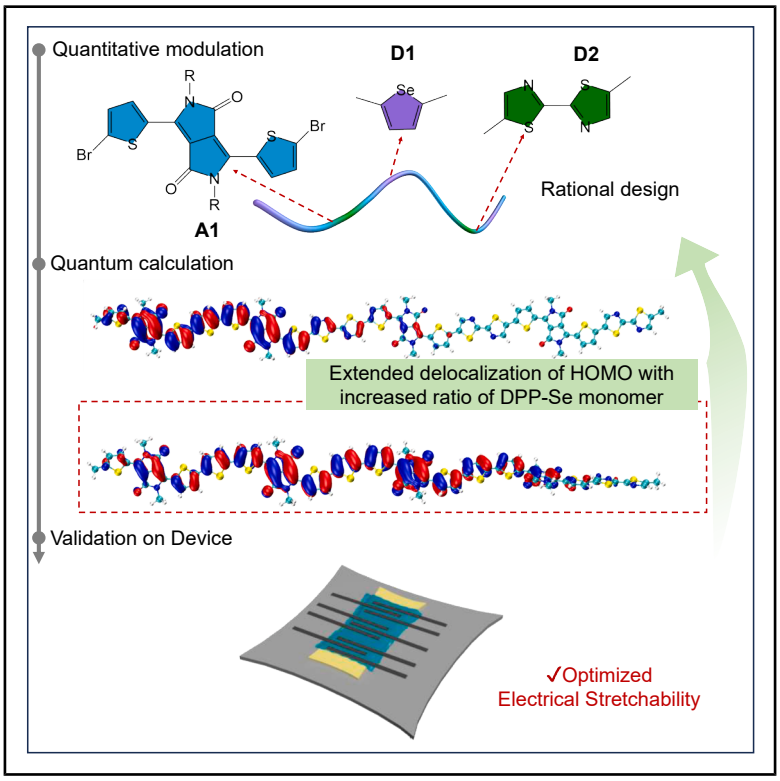

Highlights

- A novel group of stretchable semiconductors, DPP-mSe-nTz, are synthesized
- D_{del} can be a numerical descriptor to design co-monomer ratio of conjugated terpolymers
- Delocalization length of DPP-mSe-nTz increases with the ratio of DPP-Se co-monomer

Authors

Qing Zhou, Shiwei Ren, Björn Baumeier, Zhengran Yi, Yunqi Liu, Yan Zhao

Correspondence

b.baumeier@tue.nl (B.B.),
yzr@whu.edu.cn (Z.Y.),
zhaoy@fudan.edu.cn (Y.Z.)

In brief

Facing the challenge of developing high-performance stretchable semiconductors, Zhou et al. proposed a design strategy by backbone modulation toward extended frontier molecular orbital. Experiments and computational investigations demonstrate that DPP-mSe-nTz terpolymers with a high ratio of DPP-Se monomers exhibit extended delocalization length of HOMOs and superior electrical stretchability over other counterparts.

Zhou et al., 2026, Cell Reports Physical Science 7, 103176
March 18, 2026
https://doi.org/10.1016/j.xcrp.2026.103176

CellPress

Cell Reports
Physical Science

CellPress
OPEN ACCESS

Article

DPP-based terpolymers for enhanced electrical stretchability via backbone engineering toward delocalized frontier molecular orbital

Qing Zhou,[1,2] Shiwei Ren,[3] Björn Baumeier,[2,*] Zhengran Yi,[1,4,*] Yunqi Liu,[1] and Yan Zhao[1,5,*]
[1]Laboratory of Molecular Materials and Devices, Department of Materials Science, Fudan University, Shanghai 200433, P.R. China
[2]Department of Mathematics and Computer Science & Institute for Complex Molecular Systems, Eindhoven University of Technology, PO Box 513, 5600 MB Eindhoven, the Netherlands
[3]National Key Laboratory for Food Additives Assay, Gongbei Customs Technique Center, Gongbei Customs, Zhuhai 519001, P.R. China
[4]State Key Laboratory of Coatings for Advanced Equipment, College of Smart Materials and Future Energy, Fudan University, Shanghai 200433, P.R. China
[5]Lead contact
*Correspondence: b.baumeier@tue.nl (B.B.), yzr@whu.edu.cn (Z.Y.), zhaoy@fudan.edu.cn (Y.Z.)
https://doi.org/10.1016/j.xcrp.2026.103176

SUMMARY

Conjugated terpolymers emerge as promising candidates to develop wearable and stretchable electronics for the merits of mechanical stretchability and high charge mobility. Despite their potential, backbone structural diversity causes significant variability and limited predictability in their electrical stretchability, hindering their rational design. Here, we report a rational design on the backbone structure for high-performance stretchable terpolymers. We study a novel group of terpolymers, DPP-mSe-nTz, with varying ratios of two co-monomer units. The frontier molecular orbital exhibits higher delocalization length with the increased ratio of DPP-Se segments. Accordingly, terpolymers with extended frontier molecular orbital exhibit superior electrical performance under strain. The optimized terpolymer (DPP-75Se) exhibits high hole mobility of 0.29 $cm^2 V^{-1} s^{-1}$ and high retention of 28% under 100% strain. Combining observation on the morphology evolution and computational analysis of charge transport, we propose a comprehensive understanding of frontier molecular orbital delocalization in enhancing the electrical stretchability of terpolymers.

INTRODUCTION

Intrinsically stretchable polymer semiconductors hold immense promise for advancing next-generation wearable electronics, enabling the development of ultra-efficient, flexible, and miniaturized devices that seamlessly integrate with the human body.[1–7] These advancements are poised to drive innovations in healthcare,[8–12] human-machine interaction,[13–17] and the Internet of Everything.[18,19] Most semicrystalline polymer semiconductors, characterized by linearly extended π units, exhibit planarity and strong inter-molecular interactions.[20,21] The intensive π-π interactions between molecules facilitate co-facial stacking, resulting in long-range ordered structures that ensure efficient charge transport within conjugated polymer films. However, this structural rigidity also limits their stretchability and ductility, creating a fundamental challenge in simultaneously achieving high stretchability and efficient charge-transport performance.

To impart stretchability by molecular engineering, an emerging strategy is to construct a polymer backbone with alternating building blocks. Early efforts introduced flexible non-conjugated segments, such as alkyl and alkoxy groups, into the polymer backbone as conjugation break spacer.[22–26] This approach was found to lower the crystallinity and elastic modulus of conjugated polymer thin films and thus enhance their stretchability, albeit at the expense of charge-transport performance. The trade-off originates from the disruption of the regular, planar chain conformation by these single-bond linkages, which interrupts the continuous π-conjugated pathway along the backbone. To mitigate the detrimental impact of non-conjugated units on backbone conjugation, fused-ring motifs, such as indacenodithiophene and spirofluorene derivatives, were subsequently proposed as structural replacements.[27,28] This strategy enables improved mechanical compliance while better preserving charge-carrier mobility. Based on this, the terpolymer strategy was proposed, incorporating three conjugated units to form randomly co-blocked terpolymers.[29,30] This method has shown potential in reducing backbone regularity while maintaining the extended conjugated structure, which can simultaneously enhance stretchability and preserve charge-transport efficiency.

Despite the progress, the diversity in backbone structure leads to significant variability and limited predictability in the electrical stretchability, hindering the rational design of stretchable terpolymers (Table S1). Two critical issues persist: (1) selecting appropriate co-monomer units and (2) optimizing the ratio of monomer units to achieve the desired balance between

Please cite this article in press as: Zhou et al., DPP-based terpolymers for enhanced electrical stretchability via backbone engineering toward delocalized frontier molecular orbital, Cell Reports Physical Science (2026), https://doi.org/10.1016/j.xcrp.2026.103176

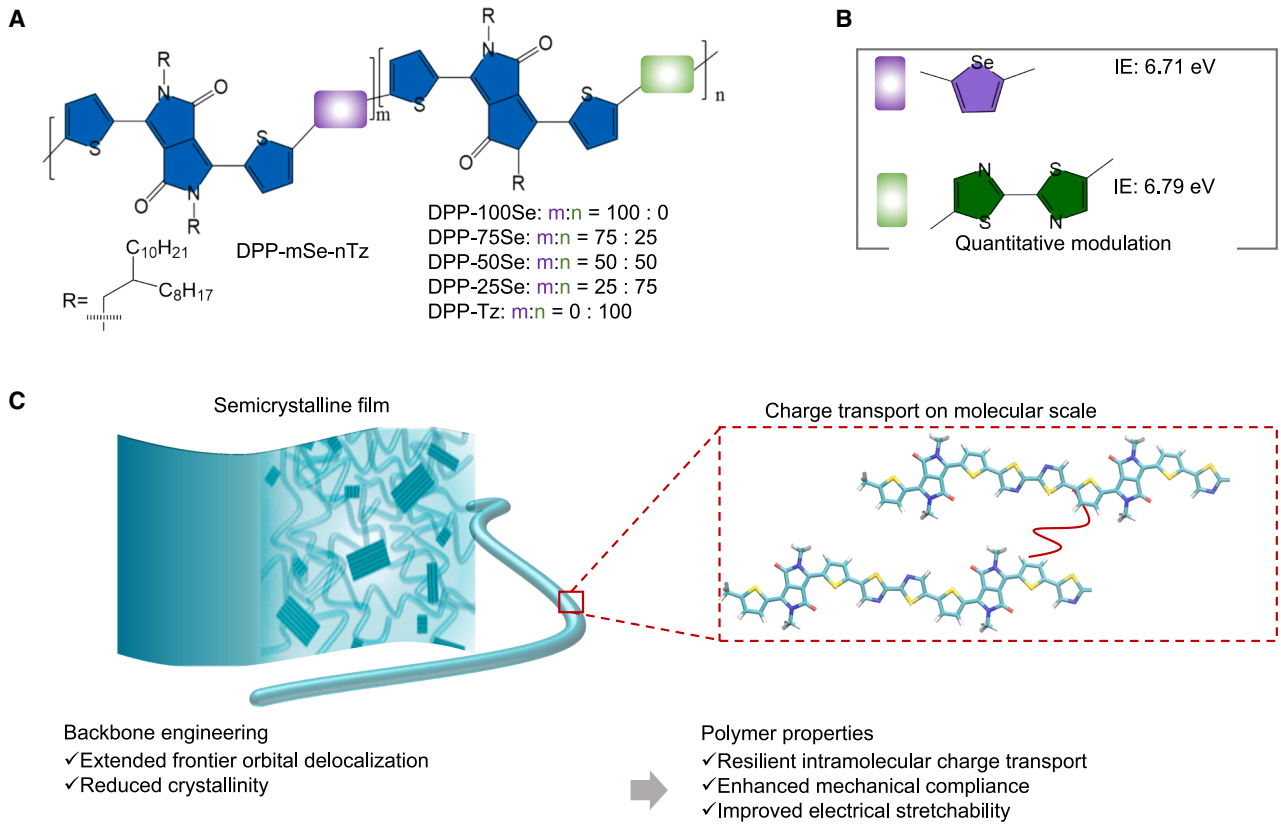

Scheme 1. Design strategy of the terpolymers

(A) Chemical structure of the terpolymer based on DPP, selenophene, and bithiazole.

(B) Calculated ionization energy of methyl-substituted selenophene and methyl-substituted bithiazole.

(C) Optimizing the electrical stretchability in terpolymers by elucidating the synergistic impact of microstructure and electronic structure.

electrical performance and stretchability. This is because no other indicator has been proposed for understanding the performance of terpolymers apart from their improved mechanical stretchability.[27,29,31,32] Instead, terpolymers were developed by a trial-and-error method. Here, we assume that frontier molecular orbital (FMO) of the terpolymers is a critical indicator for understanding the electrical performance, as it has a pivotal role that determines the charge transport on the molecular scale. Recent advancements in photovoltaic devices reveal that the electronic structure of terpolymers is highly influenced by molecular structure,[33–36] which significantly determines the device performance. However, when designing terpolymers for stretchable electronics, the impact of electronic structure has not been well understood. Documented research primarily focused on reducing the crystallinity in ternary conjugated polymer films, attributing the performance retention merely to microstructural optimization.[27] The relationship between microstructure, electronic structure, and charge-transport properties in terpolymers is not yet fully understood, complicating the selection and quantitative modulation of conjugated units. Furthermore, the conformational changes under strain significantly impact charge transport,[37–39] making it difficult to predict the electrical performance of terpolymer films during deformation. Therefore, a deeper understanding of the interplay between terpolymer backbone and overall properties is essential for advancing the design and synthesis of intrinsically stretchable high-performance polymer semiconductors.

In this work, we propose a rational design strategy to obtain high-performance stretchable semiconductors by backbone engineering toward extended FMO. Based on the terpolymer strategy, we design and synthesize terpolymers comprising diketopyrrolopyrrole (DPP) flanked by two thiophenes, selenophene (Se) and bithiazole (Tz), as model compounds. To tailor the backbone packing order and electronic structure, we quantitatively modulate the ratio of two types of co-monomer units in DPP-based terpolymers (Scheme 1). Ultraviolet-visible (UV-vis) spectroscopy, atomic force microscopy (AFM), and grazing-incidence wide-angle X-ray scattering (GIWAXS) are combined to probe the microstructural characteristics of the terpolymers. Additionally, quantum chemical calculations are carried out to explore the electronic structure of the terpolymers. The synergistic impact of electronic structure and microstructure on the electrical performance of terpolymers under strain is explored via stretchable organic transistors and computation. We reveal that the extended delocalization of highest occupied molecular orbitals (HOMOs) is vital for improving electrical stretchability in DPP-mSe-nTz terpolymers, and it can be modulated by controlling the ratio of DPP-Se segment. The optimized terpolymer

Please cite this article in press as: Zhou et al., DPP-based terpolymers for enhanced electrical stretchability via backbone engineering toward delocalized frontier molecular orbital, Cell Reports Physical Science (2026), https://doi.org/10.1016/j.xcrp.2026.103176

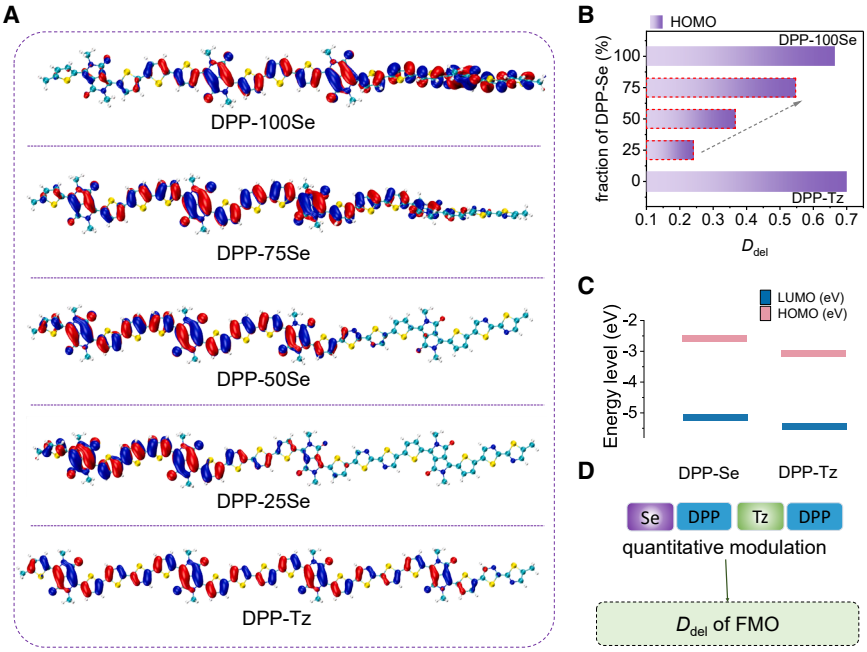

Figure 1. Calculated electronic structure of the representative oligomers

(A) Molecular structures of DPP-100Se, DPP-75Se, DPP-50Se, DPP-25Se, and DPP-Tz after optimization. The conjugated backbone and the highest occupied molecular orbital (HOMO) isosurface with a value of 0.014 a_B^{-3} is shown in each structure. The lowest unoccupied molecular orbital (LUMO) isosurface is shown in Figure S1.

(B) Degree of delocalization (D_{del}) of the HOMO state as a function of fraction of DPP-Se segment in the oligomers.

(C) Energy levels of the HOMO and LUMO of DPP-Se monomer and DPP-Tz monomer.

(D) Schematic demonstrating the dependent D_{del} of terpolymers on the ratio of monomer units. FMO, frontier molecular orbital.

(DPP-75Se) exhibits high hole mobility of 0.29 $cm^2 V^{-1} s^{-1}$ and superior electrical stretchability compared to other terpolymers, demonstrating that high charge mobility and electrical stretchability can be achieved by tuning the FMO delocalization length.

RESULTS

Molecular design

In this work, we prepared a series of DPP-based terpolymer semiconductors with varying fractions of selenophene and bithiazole. The selection of these building blocks is guided by the following considerations. (1) The parent donor-acceptor conjugated polymer DPP-Se, constructed from DPP units flanked with two thiophenes and one selenophene, exhibits favorable inter- and intra-molecular charge transport due to its coplanarity.[40,41] The high polarity of selenium facilitates strong interactions between selenium-containing moieties and oxygen in DPP units, resulting in a more planar backbone conformation that supports efficient charge transport.[42] However, such high co-planarity also leads to strong aggregation at the microscopic scale, reducing resilience under stretching and limiting electrical stretchability. (2) Incorporating bithiazole into the backbone to partially replace selenophene will (1) reduce structural regularity due to the differing ring sizes and (2) serve as an electronic equivalent to selenophene, given their comparable electron-donating effect.[43,44] This is confirmed by their similar ionization energies. As shown in Scheme 1, the calculated (via density functional theory [DFT] ΔSCF at PBE0/def2-tzvp level) ionization energies of methyl-substituted selenophene and methyl-substituted bithiazole are 6.71 eV and 6.79 eV, respectively. The terpolymers were labeled as DPP-100Se (100 mol % selenophene and 0 mol % bithiazole), DPP-75Se, DPP-50Se, DPP-25Se, and DPP-Tz (100 mol % bithiazole and 0 mol % selenophene), according to the stoichiometric ratios of the chemical equivalents of selenothiophene and bithiazole in the conjugated polymer.

Delocalization of FMOs

The impact of backbone engineering on the electronic structure was studied via computational method. Density functional theory (DFT) was used to estimate the FMOs of the five polymers. We constructed oligomers with 4 units as prototypes of the polymer segment, with the number of DPP-Se units ranging from 4 to 0 (i.e., when the number of DPP-Se segments is 4, the number of DPP-Tz segments is 0, and so forth). The side chains ($-CH_2CHC_8H_{17}C_{10}H_{21}$) were simplified as methyl for calculation efficiency. We used PBE0 functional and def2-tzvp basis set to perform the DFT calculation via the versatile object-oriented toolkit for coarse-graining applications (VOTCA) with the ORCA package.[45–48] The optimized geometry and HOMO with isosurface value of 0.014 a_B^{-3} is shown in Figure 1A.

The extension of HOMO is quantized by the degree of delocalization (D_{del}), which is estimated from the radius of gyration of molecular orbital (R_g^{MO}) and geometry (R_g^{opt}), where $D_{del} = R_g^{MO}/R_g^{opt}$. As shown in Figure 1B, D_{del} of the terpolymers differs significantly as ratios of the two co-monomer units vary. The DPP-100Se and DPP-Tz polymer exhibit HOMO isosurface across the entire backbone, demonstrating similar D_{del} of 0.66 and 0.70, respectively. For the terpolymer, the D_{del} of the HOMO varies significantly with the number of selenophene and bithiazole units. As the number of selenophene units decreases from 3 to 1, the D_{del} of the HOMO decreases linearly, with the electron mainly localized on the DPP-Se units. Thus, the introduction of the DPP-Tz unit disrupts the conjugation of the HOMO, which is likely attributed to the higher HOMO energies of the DPP-Se units. According to the calculations (Figure 1C), the HOMO energies of methyl-terminated DPP-Se and DPP-Tz monomers −5.13 eV and −5.42 eV, respectively. Upon incorporation into continuous chains, the HOMO is predominantly localized on the DPP-Se units. Thus, the D_{del} of the HOMO is related to the extension of DPP-Se segment. As a summary, the synergistic impact of energy levels of building blocks and backbone engineering on the D_{del} of terpolymers is illustrated in Figure 1D.

Please cite this article in press as: Zhou et al., DPP-based terpolymers for enhanced electrical stretchability via backbone engineering toward delocalized frontier molecular orbital, Cell Reports Physical Science (2026), https://doi.org/10.1016/j.xcrp.2026.103176

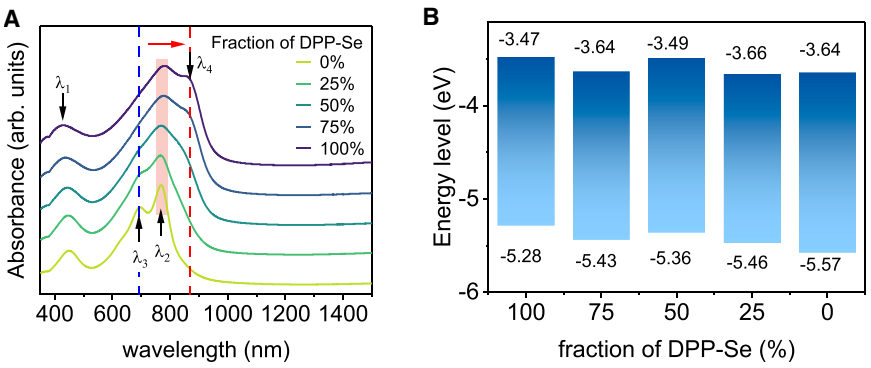

Figure 2. Optoelectrical properties of the synthesized terpolymers

(A) Normalized UV-vis absorption intensity of the five polymers. From top to bottom, the fraction of selenophene decreases from 100% to 0%.

(B) HOMO and LUMO energy levels extracted from the onset of oxidative peak and reductive peak, respectively.

Synthesis and characterizations

The terpolymers are obtained via Pd-catalyzed Stille coupling polymerization. The synthesis procedure is illustrated in Scheme S1 in supplemental methods. The results of elemental analyses and NMR spectra further confirm that the structures of the synthesized molecules were consistent with the expected compositions, with a positive correlation between the increase in the proportion of the Tz component and the proportion of N contained in the corresponding materials (Table S2 and Figures S3–S6). Especially, the characteristic peaks near 8.00 ppm correspond to two hydrogen atoms on the Tz ring, whose intensity and integral area exhibit significant response to variations in selenium content. High-temperature gel-permeation chromatography and thermogravimetric analysis results reveal that the five polymers exhibited similar molecular weight, dispersity, and thermal stability (Figure S7 and Table S2). All the polymers exhibited similar number average molecular weights (M_n) of around 50 kDa and close decomposition temperature of 350°C, which is beneficial for device processing and performance evaluation.

The optoelectrical properties of terpolymers were examined using UV-vis absorption spectroscopy and cyclic voltammetry measurements. As shown in Figure 2A, in both solution and film states, all the polymers exhibit a dual-band absorption, with identical absorption at the high-energy band (300–500 nm) and distinct absorption at the low-energy band (600–1,000 nm).[49] Two obvious shoulder peaks are observed in the lower band (λ_3, marked as blue dashed line) and higher band (λ_4, marked as red dashed line) near the main absorption of 770 nm for DPP-100Se and DPP-Tz, respectively. As the fraction of selenophene increases from 25% to 75%, a gradual increase of λ_4 is observed along with decreased λ_3, indicating a quantitative change of Se and Tz moieties within the backbones. Energy levels of HOMO and lowest unoccupied molecular orbital (LUMO) were estimated by cyclic voltammetry (Figures S8 and S9). The measured HOMO energy level of the five polymers ranges from −5.6 to −5.3 eV, typical for DPP-based polymers (Figure 2B and Table S3).

Reduced crystallinity of terpolymers

To investigate the influence of backbone structures on the overall crystallinity and packing ordering of polymers, GIWAXS was applied to the polymer films. Detailed information about the experiments is provided in the supplemental information. As shown in Figures 3A and S10, all the polymer films demonstrate edge-on dominated packing ordering, identified by signal of lamellar packing (h00) out of plane. Note that in DPP-100Se film, a board signal of (010) indicates that a minority of face-on domains coexist. AFM also confirms that all the polymer films exhibit aggregated morphology. As shown in Figures S12 and S13, the topography of all five polymer films displays pronounced aggregation features with characteristic width of about 170 nm and similar roughness. This morphology indicates a semicrystalline structure in these DPP-xSe films, which is typical for conjugated polymers. DPP-100Se and DPP-Tz films demonstrate progress of (h00) peaks with high intensity and a well-recognized (010) peak of π-π stacking at q = 1.7 Å^{-1}. These results indicate long-range backbone packing within both films. This ordered packing can be tailored by tuning the backbone regularity, as confirmed by the declining crystallinity and crystalline domain size in terpolymer films. With the decrease of the fraction of DPP-Se segment, the relative degree of the crystallinity (rDoc) demonstrates a parabolic trend, reaching its lowest value at DPP-50Se. Meanwhile, the domain size of the crystalline region is estimated from the (100) peak according to the Scherrer equation.[50] Compared to the corresponding donor-acceptor (D-A) polymers, terpolymers exhibit smaller domain size along the lamellar packing direction (around 9 nm). Among the terpolymers, DPP-75Se exhibits the smallest domain size of 7 nm on average. This indicates that in chlorobenzene, DPP-Tz segments find it easier than DPP-Se segments to form ordered aggregates. When a small fraction (25%) of bithiazole moiety is incorporated, the crystallization of the DPP-Se segment is disrupted and only short-range aggregates can be formed, as identified by the (100) signal in the GIWAXS pattern (Figure 3A). In this case, the crystalline domain exhibits a packing manner identical to that of DPP-100Se. As the fraction of DPP-Tz segments increases further, repeated segments of DPP-Tz tend to aggregate into larger sizes. The profile of GIWAXS demonstrates a clear evolution of the (h00) with the fraction of DPP-Se segment (Figure 3B). The molecular packing of polymers was also investigated, as shown in Figures 3C and S11. DPP-Tz and DPP-100Se exhibit π-π stacking distance with the value of 3.64 Å and 3.77 Å, respectively. Interestingly, π-π stacking distance in the terpolymers demonstrates a parabolic distribution instead of a linear distribution. Terpolymers are anticipated to pack in the manner of D-A

Please cite this article in press as: Zhou et al., DPP-based terpolymers for enhanced electrical stretchability via backbone engineering toward delocalized frontier molecular orbital, Cell Reports Physical Science (2026), https://doi.org/10.1016/j.xcrp.2026.103176

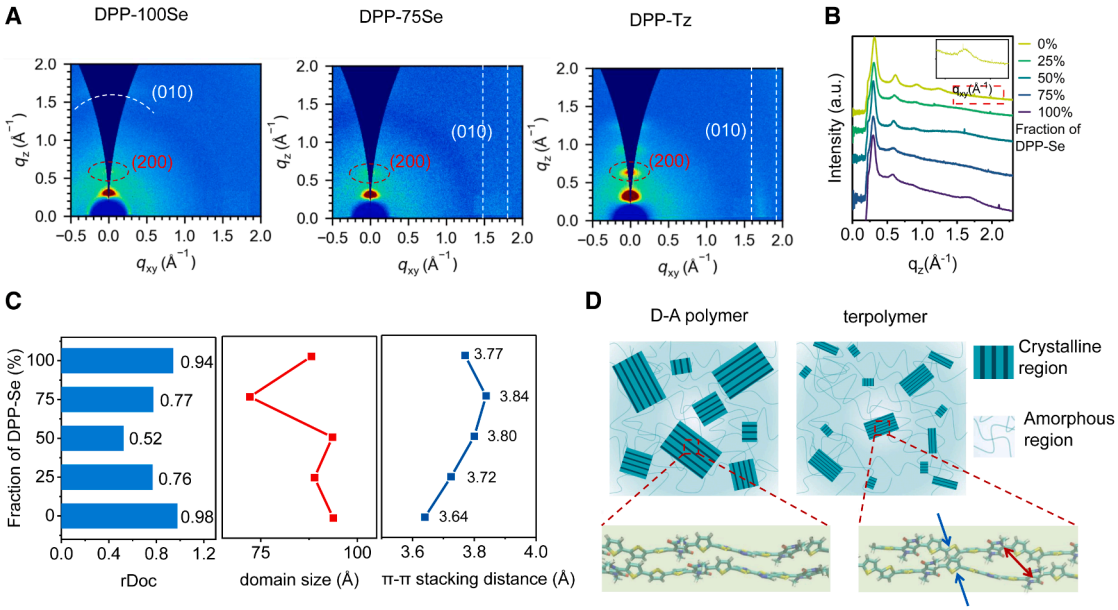

Figure 3. Impact of the backbone structures on the microstructure of polymer films

(A) GIWAXS patterns of polymer films DPP-100Se, DPP-75Se, and DPP-Tz. The GIWAXS pattern of polymer DPP-50Se and DPP-25Se are displayed in Figure S10. Lamella packing signals (200) are marked by red dashed ellipses. π-π stacking signals (010) are marked in white.

(B) Out-of-plane profiles of the corresponding GIWAXS patterns. Intensity is integral of area with $\chi = -10°$ to 10°. Inset image is the in-plane profile of DPP-Tz with integral of area with χ = 80°–90°.

(C) (Left) Relative degree of the crystallinity (rDoc), (middle) domain size of the crystalline region in the direction of lamellar packing direction, and (right) π-π stacking distance of the five polymers as a function of the fraction of DPP-Se segment. The rDoc value was extracted by calculating the peak integral of (100) and the peak integral near q = 1.4 Å^{-1} for amorphous region (rDoc = $A_{100}/A_{amorphous}$).

(D) Schematic of the crystalline domains and the corresponding molecular packing order in the D-A polymer and terpolymer.

polymers. However, owing to the steric effect between alternating units in co-facial stacked chains, as illustrated in Figure 3D, terpolymers exhibit larger π-π stacking distance than D-A polymers. These results confirm that an irregular backbone is the origin of lower crystallinity and short domain size in terpolymer films.

To study the mechanical compliance of their crystalline regions, i.e., chain mobility, GIWAXS experiments were conducted on the stretched films (Figure 4A). When subjected to tensile strain, polymer chains with higher mechanical compliance are easier to slide over to dissipate the stress, rather than breakage of the crystalline domain[51–54] (Figure 4B). Therefore, alignment of polymer backbone can be used to compare the flexibility of chains. To compare the strain-induced alignment of the crystalline domain, the incident light was aligned parallel and perpendicular to the stretching direction (Figures 4C and S15). To ensure that all the investigated films are under comparable tensile stress while similar strain is applied, we keep the five polymer films under similar crack onset strain (COS) by controlling the molecular weight (Table S2). As shown in Figure S14, all five films demonstrate similar COS (70%–80%). Figures 4C and S15 show the GIWAXS pattern of stretched DPP-mSe-nTz films. Anisotropy ratios of the (100) peak area in the two directions were calculated to quantify the chain alignment (Figure 4D). Compared to DPP-100Se and DPP-Tz, all the terpolymers demonstrate a higher anisotropic ratio after being stretched to 50% and 100% strain. Among them, DPP-75Se exhibits the highest anisotropy, likely due to the smaller domain size. When applied to 50% strain, DPP-75Se demonstrates a high anisotropic ratio of 3.33, which increases up to 4.71 when stretched to 100% strain. These results confirm that terpolymers exhibit higher chain mobility than D-A polymers. Due to their different chain mobility, the microstructure evolves differently to dissipate the strain energy. When subjected to strain, crystalline domains with large size tend to break to dissipate the strain energy, while short-range ordered aggregates exhibit higher mobility to adjust the tension and retain the ordered structure upon large strain.

Meanwhile, the lamellar packing distance (*d-d* spacing distance) in the terpolymers demonstrates a different trend compared with the binary D-A polymers. As displayed in Table 1, *d-d* spacing distance increased by ~0.7 Å and 1.1 Å in DPP-100Se and DPP-Tz, respectively, while the films were under 50% strain, and this strain-induced expansion remained obvious even upon strain increase to 100%. This observation is consistent with other reported DPP-based binary conjugated polymers under strain, which is thought to be the morphological response of edge-on domains to the in-plane stretching stress.[37,38] In contrast, *d-d* spacing distance in the three terpolymers decreased by ~0.5 Å as the strain increased to 50%, and this declining effect remained obvious even upon strain increase to 100%. These results indicate that backbone rigidity has remarkable influence on the morphological responses of domains to stretching stress in terpolymer films and binary polymer films.

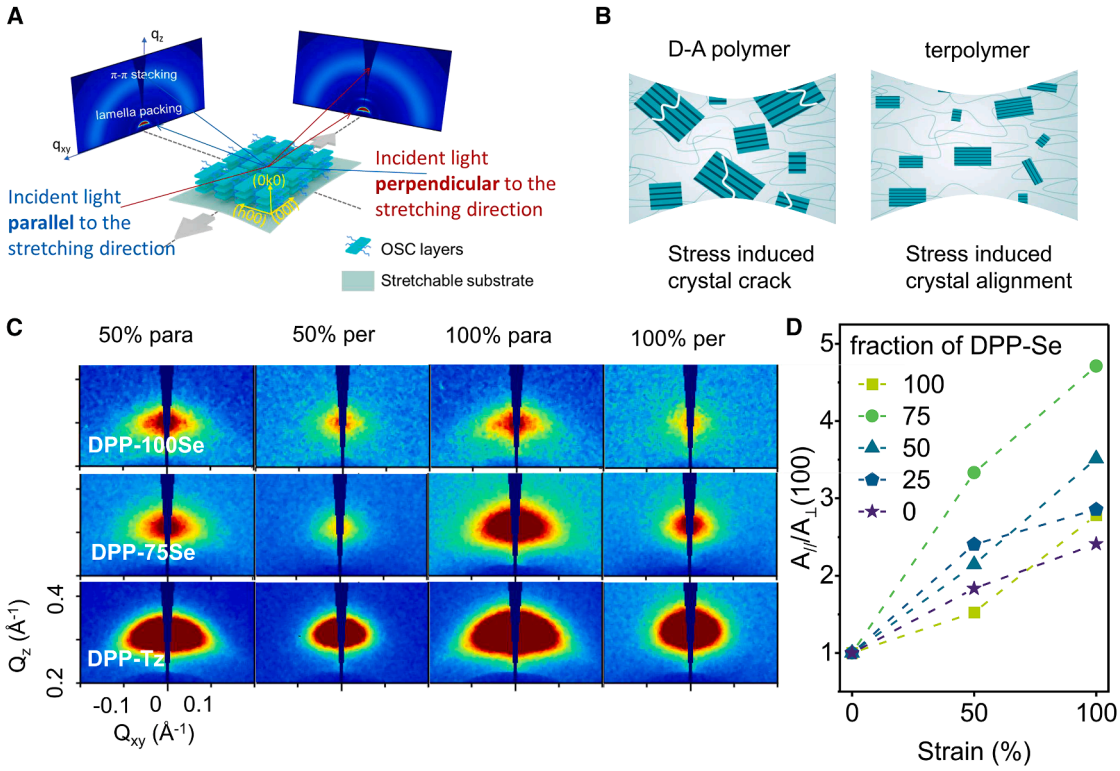

Figure 4. Impact of the terpolymer strategy on the microstructure of polymer films under strain

(A) Schematic illustrating GIWAXS analysis of the stretched semiconductors.

(B) Schematic illustrating the crystalline domains deformed in the stretched D-A polymer film and the terpolymer films, respectively.

(C) Images of the GIWAXS of polymer films under strain. 50% and 100% denote that the films were stretched to 50% strain and 100% strain. Para and per denote that the incident light was parallel to and perpendicular to the stretching direction.

(D) Ratio of peak integral of (100) for the same sample when the incident light was parallel to and perpendicular to the stretching direction.

Electrical performance of the stretchable OFETs

To confirm the impact of D_{del} of HOMO on the electrical performance of all the terpolymers, we fabricated OFETs on rigid and stretchable substrates. First, OFETs with a bottom-gate, bottom-contact structure were fabricated on Si/SiO_2 substrates to characterize the inherent electrical performance. Figure 5A shows an optical image and the structure of the devices. As shown in Figures 5B and 5C, all devices exhibited hole-dominant transport characteristics, with on/off ratios exceeding 10^3 and on-state current reaching 10 μA. These results indicate that OFETs using DPP-mSe-nTz conjugated polymers as the active layer exhibit good performance. The device parameters are summarized in Table S5. DPP-100Se exhibits the highest mobility of 0.31 $cm^2\ V^{-1}\ s^{-1}$, while the OFET with DPP-Tz as the hole-transporting layer shows a lower mobility of 0.080 $cm^2\ V^{-1}\ s^{-1}$. Compared with DPP-100Se, DPP-75Se retained a hole mobility of 93% (0.29 $cm^2\ V^{-1}\ s^{-1}$), while DPP-50Se retained a hole mobility of 0.12 $cm^2\ V^{-1}\ s^{-1}$. Further increasing the bithiazole content to 75% led to a drastic reduction in the hole mobility of DPP-25Se to 0.020 $cm^2\ V^{-1}\ s^{-1}$. According to previous research, the carrier mobility of ternary conjugated polymers is usually significantly attenuated compared to its binary conjugated polymers. It is generally believed that this performance degradation is caused by decreased crystallinity.[23] However, the mobility observed among terpolymers in our study shows different trends from rDoc obtained from GIWAXS

Table 1. Lamellar packing distance—*d-d* spacing distance, in angstroms—under strain in DPP-mSe-nTz polymer films

		Strain = 50%		Strain = 100%	
Sample	Initial	Parallel	Perpendicular	Parallel	Perpendicular
DPP-100Se	21.22	21.97	21.92	22.00	21.50
DPP-75Se	20.92	20.45	20.41	20.50	20.40
DPP-50Se	20.97	20.65	20.51	20.60	20.45
DPP-25Se	20.40	20.0	19.76	20.09	20.01
DPP-Tz	19.94	21.03	20.75	20.70	20.07

Cell Reports
Physical Science
Article

CellPress
OPEN ACCESS

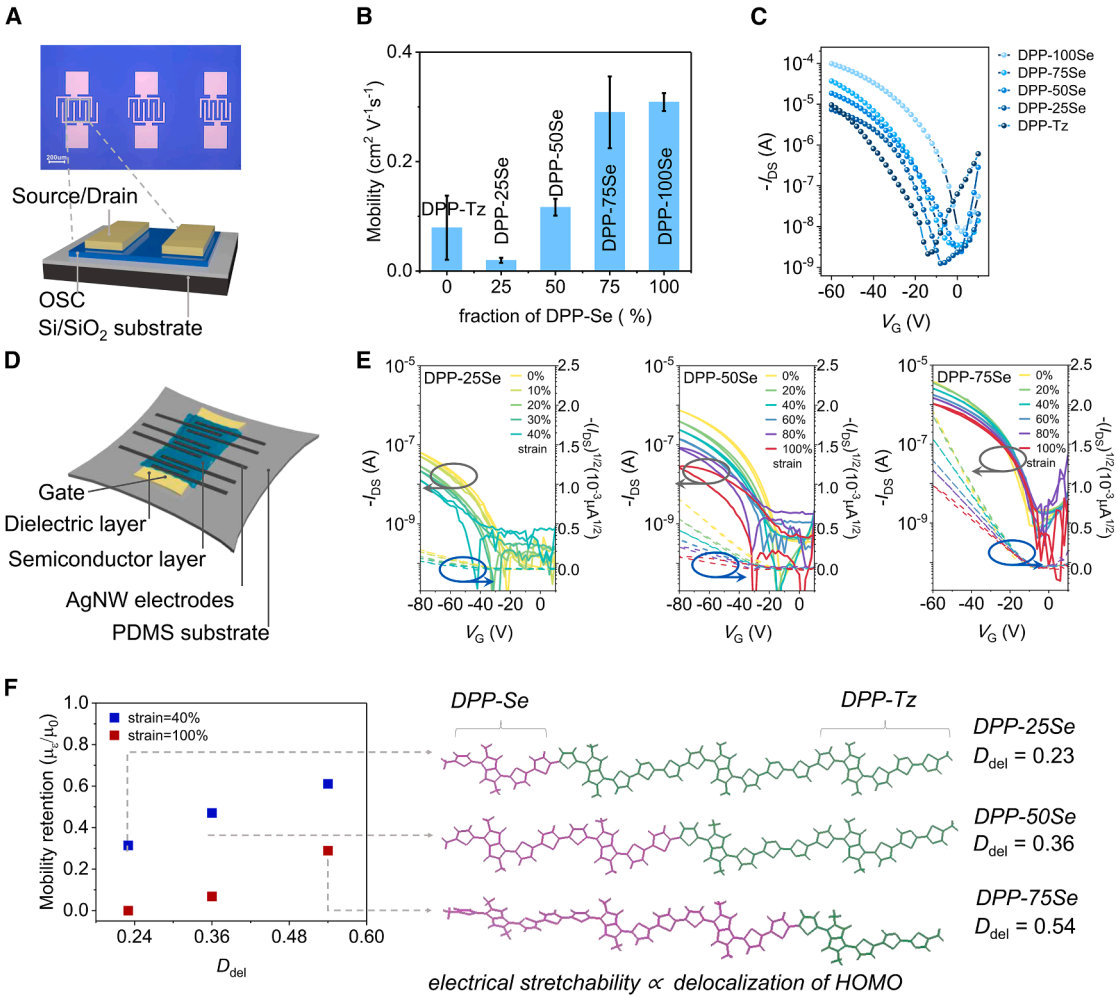

Figure 5. Electrical performance of the five polymers cooperating in field-effect transistors

(A–C) Electrical performance evaluated in rigid devices.

(A) Optical images of the devices on the Si/SiO_2 substrates and the illustration of the device structure.

(B) Mobility of the five polymers obtained from devices demonstrated in (A). For each polymer, mobility is averaged from three measurements in three devices with channel length of 30 μm and channel width of 1,500 μm. Data are presented as mean ± standard deviation. Representative transfer curves for each polymer are displayed in Figures S16–S21.

(C) Comparison of the typical transfer curves of the corresponding devices. $V_{DS} = -60$ V.

(D–F) Electrical performance evaluated in fully stretchable OFETs.

(D) Illustration of the fully stretchable OEFT.

(E) Comparison of the transfer curves of stretchable OFETs employing different DPP-xSe terpolymer (left: DPP-25Se; middle: DPP-50Se; right: DPP-75Se) as the semiconducting layers. For all the devices, the transfer curves were measured from 0% to 100% strain with interval of 20% strain, except for the DPP-25Se, where the devices failed after being stretched to 40% strain. $V_{DS} = -60$ V. Due to the difference in V_{th}, drain current for the DPP-100Se device and the DPP-75Se device was measured with V_G ranging from −60 to 10 V, while for other devices the drain current was measured with V_G ranging from −80 to 10 V.

(F) Mobility retention of DPP-xSe terpolymers with respect to the delocalization of HOMO under strain 40% (blue squares) and 100% (red squares). The corresponding transfer curves for each device under strain are displayed in Figure S22 and in (E). Detailed parameters are summarized in Tables S5–S9.

measurements, where the DPP-25Se exhibits comparable rDoc with DPP-75Se but much lower charge mobility. This can be explained by the localized HOMO on the DPP-Se segment in DPP-25Se, because the extending HOMO is advantageous both to charge transport along the backbone direction and to inter-molecular transport. The stability of the terpolymers was also investigated (Figure S21). After storage in ambient environment for 5 months, all polymers exhibited degraded charge mobility. Among them, DPP-100Se demonstrated the best stability, with mobility of 55%.

The delocalization of HOMO also demonstrates significant influence on the electrical performance of terpolymers in stretchable OFETs. As illustrated in Figure 5D, fully stretchable OFETs with bottom gate and top gate were fabricated to investigate their electrical stretchability. The fabrication of the fully stretchable OFETs is detailed in the supplemental information. At initial

Please cite this article in press as: Zhou et al., DPP-based terpolymers for enhanced electrical stretchability via backbone engineering toward delocalized frontier molecular orbital, Cell Reports Physical Science (2026), https://doi.org/10.1016/j.xcrp.2026.103176

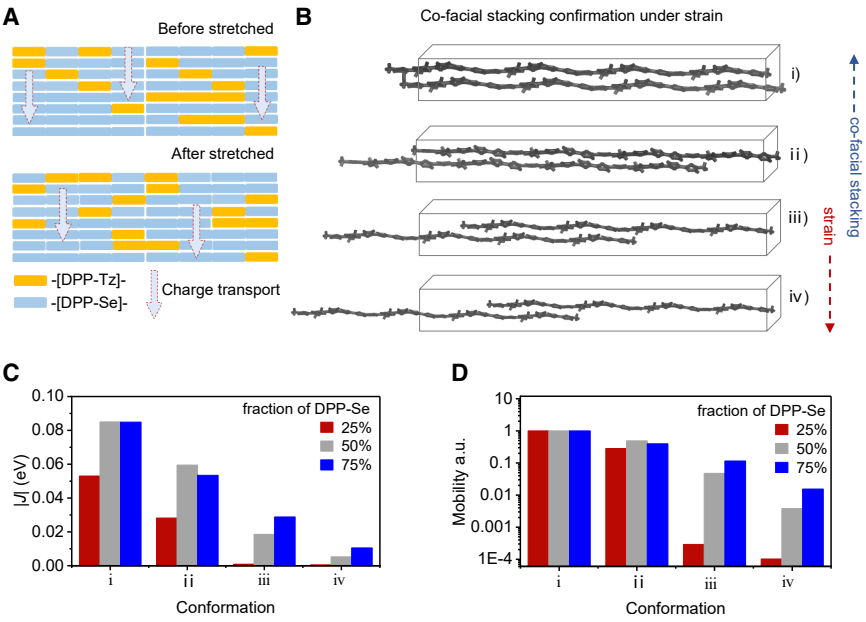

Figure 6. Calculated mobility of oligomers under strain-induced confirmation changes

(A) Illustration of charge transport in the strain-induced terpolymers. Segments shift between each other within adjacent packing chains.

(B) Co-facial stacking conformation under strain.

(C) The absolute value of calculated transfer integrals of the pairs in (B) for the oligomers with the fraction of DPP-Se segment ranging from 25% to 75%.

(D) Scaled mobilities of the pairs in (B) for the oligomers with DPP-Se segment ranging from 25% to 75%. Mobilities of different conformations are normalized to that of conformation (Bi) for each ternary polymer. The absolute values of mobility are listed in Table S3.

state, all stretchable OFETs display nearly hysteresis-free transfer curves and high on/off ratios (10^2–10^3), indicating good device performance (Figures 5E and S22). These stretchable devices exhibit hole-dominated charge transport, although their hole mobility is slightly lower than that of the rigid-substrate devices, due to the lower capacitance of the SEBS dielectric layer. Device parameters were calculated and are summarized in Tables S4–S8.

As demonstrated in Figure 5E, the electrical stretchability of terpolymer varies significantly with the ratio of selenophene to bithiazole. Before stretching, DPP-75Se exhibits charge mobility comparable with that of DPP-100Se. Under 40% strain, DPP-75Se retains 61% of its initial mobility, and this retention remains 28% under 100% strain. Compared to DPP-75Se, DPP-50Se performs worse, with a mobility retention of merely 2.6% under 100% strain. DPP-25Se has the lowest initial mobility and the worst stretchability, failing at strains above 40%, with a drain current retention of only 19% before failure. The trend in electrical stretchability among the terpolymers is consistent with the D_{del} of the terpolymers, as demonstrated in Figure 5F. A terpolymer with extended D_{del} exhibits stable mobility under conformation variations, while a terpolymer with short D_{del} demonstrates susceptible charge transport under inter-chain deformation. These results emphasize the important role of D_{del} in determining the electrical stretchability of terpolymers.

Meanwhile, DPP-75Se retains higher mobility compared to DPP-100Se and DPP-Tz. Under 100% strain, the mobility retention of DPP-100Se and DPP-Tz are 3% and 13%, respectively, whereas DPP-75Se achieves a significant improvement to 28%. This is attributed to the microstructure and electronic structure of DPP-75Se, where the improved chain mobility enables adaptive deformation to dissipate the strain energy, while the extended D_{del} preserves effective charge percolation through the film. This result demonstrates that by modulating the ratio of selenophene/bithiazole units, a terpolymer with both high mobility and enhanced electrical stretchability can be achieved.

Charge transport in the morphable network

Charge transport mainly resides along backbones (intra-molecule part) and via π-π stacking (inter-molecule part). One question concerns which part is the rate-determining part under strain. GIWAXS data suggest that the polymer backbones align along the stretching direction, indicating that short-range crystalline domains "slide" over each other to adjust their location. This movement offsets or disrupts initial co-facial stacking between adjacent crystalline domains and regenerates some new inter-chain contact, resulting in a morphable network for charge transport, as illustrated in Figure 6A. During this phase, the intra-molecular part with strong coupling will be much less affected by the structural variations. However, charge transport along π-π stacking (inter-molecule part) is more sensitive to strain and should be focused upon in the prediction model.

Here, the offset, dissociation, and regeneration of co-facial stacking between adjacent crystalline domains are described by the co-facial dimers with different overlap, as illustrated in Figure 6B. The co-facial stacking distance is set as 3.8 Å for all the terpolymers. In Figure 6B, from top to bottom, the overlap between the co-facially stacked molecules decreases from four co-monomer units to one. This model simplifies the complex structure in the films under strain by excluding, for example, the amorphous region and local structure reorganization. However, it emphasizes the key point of morphology under strain, the overlap between interfacial molecules from adjacent crystalline domains. Basically, four conformations co-exist in the films, but their ratios change with strain. Assuming that a weighted average of mobility from the four scenarios represents the overall efficiency of inter-crystal charge transport, the weight of scenario (iv) increases with strain while that of scenario (i) decreases. Thus, the calculated mobility of different scenarios can be used to predict the electrical stability of terpolymers.

According to previous research,[41,55] both DPP-Tz and DPP-Se exhibited hole charge transport. Thus, using holes as the charge carriers of the terpolymer, we calculated the corresponding transfer integral using the dimer-projection method and

mobility based on the shifting model.[56] Figure 6C presents the magnitude of the transfer integrals of three terpolymers under conformations (i) to (iv). As the overlap length decreases, transfer integrals of all terpolymers gradually decline. However, the transfer integral of DPP-75Se consistently maintains the highest transfer integral across all four conformations. Even in conformation (iv), the transfer integral of DPP-75Se remains as high as 11 meV, significantly exceeding those of DPP-50Se and DPP-25Se. In contrast, the transfer integral of DPP-25Se is consistently much lower than those of DPP-50Se and DPP-75Se across all four conformations. The significant difference in transfer integral is attributed to the different D_{del}, where longer D_{del} enables effective electronic coupling in terpolymers even if the backbones overlap poorly.

Based on the obtained transfer integral and reorganization energy (Figure S24), the charge-carrier mobility was calculated according to Marcus theory (Equation 1). Here, the influence of tensile strain on the reorganization energy is not considered.

$$\mu = \frac{wd^2}{k_B T} = \frac{J^2 d^2}{\hbar k_B T}\sqrt{\frac{\pi}{k_B T \lambda}}\exp\left[-\frac{\lambda}{4k_B T}\right]. \quad \text{(Equation 1)}$$

Here, k_B is the Boltzmann constant, T is the temperature (in kelvin), ω is the hopping rate, J is the transfer integral, $\hbar$ is the reduced Planck constant, and λ is the reorganization energy. Since the calculation does not consider the influence of the system's potential energy change (ΔG) on charge-carrier transport, the absolute values of the calculated mobilities have no direct reference significance. However, qualitative trends in the electrical performance of the respective systems arising from strain-induced structural changes are well reflected by Equation 1.

The charge mobility in the prototype models exhibits a trend similar to that of the transfer integral (Figure 6D). For each terpolymer, the mobility consistently decreases with the overlap. In conformations (i) and (ii), the mobilities of the three molecules are comparable, although those of DPP-75Se and DPP-50Se are slightly higher than that of DPP-25Se. However, in conformations (iii) and (iv), DPP-75Se exhibits a significantly higher mobility retention compared to the other two molecules. Particularly, in comparison to DPP-25Se, DPP-75Se demonstrates a mobility retention over 100 times greater. The calculation result is qualitatively consistent with the experimental results in Figure 5. The significant difference between DPP-75Se and DPP-25Se is attributed to the sensitivity of inter-molecular coupling over dimer stacking alterations. Large D_{del} enables DPP-75Se with effective electronic coupling even under short co-planar stacking. Vice versa, DPP-25Se with small D_{del} is very sensitive to dimer packing conformation. Thereby, DPP-75Se demonstrates much more stable electrical performance under strain.

By quantifying the charge transport between short-range ordered domains using the dimer models, we revealed that D_{del} determines inter-molecular charge transport in terpolymers under strain and, accordingly, the overall electrical stretchability. In the reported ternary conjugated systems for stretchable electronics,[27–30] the superior stretchability of terpolymers over their binary counterparts has largely been attributed to the increased flexibility of the resulting films. However, the performance differences among terpolymers with different component ratios remain poorly understood. In this work, we provide a mechanistic explanation from the perspectives of chain dynamics under strain and charge transport on the molecular scale, underscoring the relationship between co-monomer ratio and electronic structure. For the purpose of precision synthesis, D_{del} offers a useful guideline for pre-screening the types and ratios of co-monomers, thereby improving synthesis efficiency.

DISCUSSION

We propose a strategy that extends frontier orbital delocalization in conjugated terpolymers to develop high-performance stretchable semiconducting polymers. We synthesize a group of DPP-mSe-nTz terpolymers and investigate the influences of their backbone structures on the microstructure, electronic structure, and electrical stretchability. Experimental and theoretical analyses reveal that degree of frontier orbital delocalization increases with the ratio of DPP-Se segments, leading to enhanced electrical stretchability. The optimized terpolymer DPP-75Se (with fraction of selenophene 75%) exhibits high hole mobility of 0.29 $cm^2\ V^{-1}\ s^{-1}$ and improved electrical stretchability compared to D-A polymers and other terpolymers (DPP-25Se and DPP-50Se). These findings underscore the frontier orbital delocalization as a critical feature in the rational design of high-performance terpolymers for stretchable electronics and reveal that it can be tuned through properly controlling the ratio of building blocks in terpolymers.

METHODS

Synthesis of DPP-50Se polymer

To a pre-dried 50-mL Schlenk tube, DPP-C_8C_{10}-2Br (291.1 mg, 0.285 mmol), Se-Sn (65.0 mg, 0.142 mmol, 0.5 equiv), Tz-Sn (70.0 mg, 0.142 mmol, 0.5 equiv), and Tri(*o*-tolyl)phosphine (P(*o*-tol)$_3$, 5.2 mg, 8%) were added, followed by the addition of dry chlorobenzene through a syringe, and vented to argon for 0.5 h to adequately remove oxygen from the system. Tris(dibenzylideneacetone)dipalladium ($Pd_2(dba)_3$, 2.6 mg, 2%) was rapidly poured into the mixture, and the polymerization reaction was stirred for 3 days at 130°C before gradually returning to room temperature. The mixture was added dropwise by pipette to 200 mL of methanol solution accompanied by rapid generation and precipitation of solids. The precipitate was purified by Soxhlet extraction with methanol (12 h), acetone (12 h), and hexane (12 h) and finally collected in chloroform. The resulting solution was concentrated and precipitated into methanol. The precipitate was then collected by filtration and dried under high vacuum for 5 h (80°C) overnight. The final product was in the form of a dark powder with a yield of 84.9%.

The other four polymers were synthesized under similar reaction conditions and purification procedures except for the initial monomer feed ratios. The corresponding yields were, in order, as follows: 89.5% for DPP-100Se, 85.1% for DPP-75Se, 86.5% for DPP-25Se, and 90.2% for DPP-Tz. More details about

the substances we utilized in this procedure are provided in the supplemental information.

Construction of fully stretchable OFETs

The fully stretchable OFETs were fabricated by utilizing the polydimethylsiloxane (PDMS) substrate to pick up the upper layers in the order gate electrode, dielectric layer, semiconducting polymer films, and source and drain electrodes. More details can be found in the supplemental information.

Construction of rigid devices

The rigid field-effect transistors were fabricated on the Si/SiO_2 with a bottom-gate-top-contact structure. First, the Si/SiO_2 substrates were treated with O_2 plasma for 2 min and then modified with octadecyltrichlorosilane (OTS) solution (diluted using *n*-hexane, OTS/*n*-hexane [v/v] = 1:200) for 60 s. The semiconducting polymer solutions were then cast on the Si/SiO_2 substrates and annealed in a N_2 glovebox for 30 min. Finally, the Au was fabricated on the semiconducting polymer layers through thermal evaporation. The thickness of Au electrodes was 40 nm. The channel width was 1,500 μm and the channel length 30 μm and 50 μm, respectively.

Electrical characterization of OFETs on Si/SiO_2 substrate

To evaluate the electrical performance of the investigated conjugated polymer films on silicon wafers, bottom-gate-top-contact field-effect transistors were fabricated by directly spin-coating semiconducting films on top of OTS-modified 300-nm-SiO_2/Si, then Au (30 nm) was evaporated as the source and drain electrodes. The channel length (L) and width (W) were 30 μm and 1,500 μm, respectively. The electrical performance of transistors was measured with Keithley-4200 in the glovebox. The field-effect hole mobility μ was calculated in the saturation regime of transistor operation from the equation

$$\mu_{sat} = \left(\frac{\partial\sqrt{I_{DS}}}{\partial\sqrt{V_{GS}}}\right)^2 * \left(\frac{2L}{WC_i}\right), \qquad \text{(Equation 2)}$$

where μ_{sat} is the saturation mobility, I_{DS} is the drain-source current, V_{GS} is the gate voltage, V_{DS} is the drain-source voltage, C_i is the capacitance per unit area, L is the channel length, and W is the channel width. For both the OFETs on Si/SiO_2 substrates and stretchable substrates, we extracted the saturation mobilities from transfer curves in saturated regions (V_{DS} = −50 to −60 V, V_{GS} sweeps from 0 V to 60 V).

Electrical characterization of stretchable OFETs

All the characterizations of stretchable OFETs were the same as those measured on the OFETs on Si/SiO_2 substrates, except that the mobilities were calculated with consideration of the device geometry change and dielectric capacitance (Table S11).

Material characterizations

The material structures were characterized via UV-vis absorption, GIWAXS, AFM, and optical microscopy. The supporting information provides more details. The data used to plot figures in the main text are summarized in Data S1.

RESOURCE AVAILABILITY

Lead contact

Requests for further information and resources should be directed to and will be fulfilled by the lead contact, Yan Zhao (zhaoy@fudan.edu.cn).

Materials availability

All unique/stable reagents generated in this study are available from the lead contact with a completed materials transfer agreement.

Data and code availability

- All data reported in this paper will be shared by the lead contact upon request.
- The codes for calculation used in this work can be accessed from https://www.votca.org/.
- Any additional information required to reanalyze the data reported in this paper are available from the lead contact upon request.

ACKNOWLEDGMENTS

This research was financially supported by the National Natural Science Foundation of China (52473297 and T2441002). The authors thank beamline BL14B1/15U of the Shanghai Synchrotron Radiation Facility (SSRF, China) for providing the beam time and for their assistance during experiments.

AUTHOR CONTRIBUTIONS

Conceptualization, Q.Z., B.B., Y.Z., and Z.Y.; methodology, B.B., Y.Z., and Z.Y.; investigation, Q.Z. (fabricated the devices, performed the electrical measurement and material structure characterization, and conducted the theoretical calculations) and S.R. (synthesized the semiconducting polymers and performed the material structure characterization); formal analysis, Q.Z. and S.R.; data curation, Q.Z. and S.R.; writing – original draft, Q.Z.; writing – review & editing, B.B., Z.Y., Y.Z., and S.R.; funding acquisition, Y.Z. and Y.L.; resources, Y.L. and B.B.; and supervision, B.B., Z.Y., Y.Z., and Y.L. All authors reviewed and commented on the manuscript.

DECLARATION OF INTERESTS

The authors declare no competing interests.

SUPPLEMENTAL INFORMATION

Supplemental information can be found online at https://doi.org/10.1016/j.xcrp.2026.103176.

Received: October 28, 2025
Revised: December 21, 2025
Accepted: February 12, 2026

REFERENCES

1. Cai, Y.W., Zhang, X.N., Wang, G.G., Li, G.Z., Zhao, D.Q., Sun, N., Li, F., Zhang, H.Y., Han, J.C., and Yang, Y. (2021). A flexible ultra-sensitive triboelectric tactile sensor of wrinkled PDMS/MXene composite films for E-skin. Nano Energy *81*, 105663.
2. Boutry, C.M., Negre, M., Jorda, M., Vardoulis, O., Chortos, A., Khatib, O., and Bao, Z. (2018). A hierarchically patterned, bioinspired e-skin able to detect the direction of applied pressure for robotics. Sci. Robot. *3*, eaau6914.

3. Yang, K., Li, Q., Tian, S., Wang, J., Lu, G., Guo, H., Xu, S., Zhang, L., and Yang, J. (2024). Highly Stretchable, Self-Healing, and Sensitive E-Skins at-78 °C for Polar Exploration. J. Am. Chem. Soc. *146*, 10699–10707.
4. Jager, E.W., Smela, E., and Inganäs, O. (2000). Microfabricating conjugated polymer actuators. Science *290*, 1540–1545.
5. Wang, W., Jiang, Y., Zhong, D., Zhang, Z., Choudhury, S., Lai, J.C., Gong, H., Niu, S., Yan, X., Zheng, Y., et al. (2023). Neuromorphic sensorimotor loop embodied by monolithically integrated, low-voltage, soft e-skin. Science *380*, 735–742.
6. Wang, S., Xu, J., Wang, W., Wang, G.J.N., Rastak, R., Molina-Lopez, F., Chung, J.W., Niu, S., Feig, V.R., Lopez, J., et al. (2018). Skin electronics from scalable fabrication of an intrinsically stretchable transistor array. Nature *555*, 83–88.
7. Hu, D., Giorgio-Serchi, F., Zhang, S., and Yang, Y. (2023). Stretchable e-skin and transformer enable high-resolution morphological reconstruction for soft robots. Nat. Mach. Intell. *5*, 261–272.
8. Li, J., Liu, Y., Yuan, L., Zhang, B., Bishop, E.S., Wang, K., Tang, J., Zheng, Y.Q., Xu, W., Niu, S., et al. (2022). A tissue-like neurotransmitter sensor for the brain and gut. Nature *606*, 94–101.
9. Nakatsuka, N., Yang, K.A., Abendroth, J.M., Cheung, K.M., Xu, X., Yang, H., Zhao, C., Zhu, B., Rim, Y.S., Yang, Y., et al. (2018). Aptamer–field-effect transistors overcome Debye length limitations for small-molecule sensing. Science *362*, 319–324.
10. Wang, Y., Qian, Y., Zhang, L., Zhang, Z., Chen, S., Liu, J., He, X., and Tian, Y. (2023). Conductive metal–organic framework microelectrodes regulated by conjugated molecular wires for monitoring of dopamine in the mouse brain. J. Am. Chem. Soc. *145*, 2118–2126.
11. Zhao, C., Cheung, K.M., Huang, I.W., Yang, H., Nakatsuka, N., Liu, W., Cao, Y., Man, T., Weiss, P.S., Monbouquette, H.G., and Andrews, A.M. (2021). Implantable aptamer–field-effect transistor neuroprobes for in vivo neurotransmitter monitoring. Sci. Adv. *7*, eabj7422.
12. Xu, C., Wu, F., Yu, P., and Mao, L. (2019). In vivo electrochemical sensors for neurochemicals: recent update. ACS Sens. *4*, 3102–3118.
13. Yan, H., Chen, Z., Zheng, Y., Newman, C., Quinn, J.R., Dötz, F., Kastler, M., and Facchetti, A. (2009). A high-mobility electron-transporting polymer for printed transistors. Nature *457*, 679–686.
14. Yuan, R., Tiw, P.J., Cai, L., Yang, Z., Liu, C., Zhang, T., Ge, C., Huang, R., and Yang, Y. (2023). A neuromorphic physiological signal processing system based on VO2 memristor for next-generation human-machine interface. Nat. Commun. *14*, 3695.
15. Vaghasiya, J.V., Mayorga-Martinez, C.C., Vyskočil, J., and Pumera, M. (2023). Black phosphorous-based human-machine communication interface. Nat. Commun. *14*, 2.
16. Yuk, H., Wu, J., and Zhao, X. (2022). Hydrogel interfaces for merging humans and machines. Nat. Rev. Mater. *7*, 935–952.
17. An, S., Zhu, H., Guo, C., Fu, B., Song, C., Tao, P., Shang, W., and Deng, T. (2022). Noncontact human-machine interaction based on hand-responsive infrared structural color. Nat. Commun. *13*, 1446.
18. Masoud, M., Jaradat, Y., Manasrah, A., and Jannoud, I. (2019). Sensors of smart devices in the internet of everything (IoE) era: big opportunities and massive doubts. J. Sens. *2019*, 1–26.
19. Portilla, L., Loganathan, K., Faber, H., Eid, A., Hester, J.G., Tentzeris, M.M., Fattori, M., Cantatore, E., Jiang, C., Nathan, A., and Fiori, G. (2023). Wirelessly powered large-area electronics for the Internet of Things. Nat. Electron. *6*, 10–17.
20. Printz, A.D., and Lipomi, D.J. (2016). Competition between deformability and charge transport in semiconducting polymers for flexible and stretchable electronics. Appl. Phys. Rev. *3*, 021302.
21. Yang, L., Wu, Y., Yan, Y., Wang, Z., Qiao, Y., Chang, D., Zhang, C., Wang, Y., Lu, X., Liu, Y., and Zhao, Y. (2022). Molecular packing and charge transport behaviors of semiconducting polymers over a wide temperature range. Adv. Funct. Mater. *32*, 2202456.
22. Peng, R., Pang, B., Hu, D., Chen, M., Zhang, G., Wang, X., Lu, H., Cho, K., and Qiu, L. (2015). An ABA triblock copolymer strategy for intrinsically stretchable semiconductors. J. Mater. Chem. C Mater. *3*, 3599–3606.
23. Mun, J., Wang, G.N., Oh, J.Y., Katsumata, T., Lee, F.L., Kang, J., Wu, H., Lissel, F., Rondeau-Gagné, S., Tok, J.B., and Bao, Z. (2018). Effect of nonconjugated spacers on mechanical properties of semiconducting polymers for stretchable transistors. Adv. Funct. Mater. *28*, 1804222.
24. Ji, D., Yoon, S.Y., Jeon, S., Go, J., Byeon, G., Choi, J.O., Min, J., Kim, Y., Hwang, D., Cho, K., et al. (2023). Tuning of the stretchability and charge transport of bis-diketopyrrolopyrrole and carbazole-based thermoplastic soft semiconductors by modulating soft segment contents. Adv. Mater. Interfaces *10*, 2202186.
25. Savagatrup, S., Zhao, X., Chan, E., Mei, J., and Lipomi, D.J. (2016). Effect of broken conjugation on the stretchability of semiconducting polymers. Macromol. Rapid Commun. *37*, 1623–1628.
26. Lin, Y.-C., Matsuda, M., Chen, C.K., Yang, W.C., Chueh, C.C., Higashihara, T., and Chen, W.C. (2021). Investigation of the mobility–stretchability properties of naphthalenediimide-based conjugated random terpolymers with a functionalized conjugation break spacer. Macromolecules *54*, 7388–7399.
27. Liu, D., Mun, J., Chen, G., Schuster, N.J., Wang, W., Zheng, Y., Nikzad, S., Lai, J.C., Wu, Y., Zhong, D., et al. (2021). A design strategy for intrinsically stretchable high-performance polymer semiconductors: Incorporating conjugated rigid fused-rings with bulky side groups. J. Am. Chem. Soc. *143*, 11679–11689.
28. Yu, X., Chen, L., Li, C., Gao, C., Xue, X., Zhang, X., Zhang, G., and Zhang, D. (2023). Intrinsically stretchable polymer semiconductors with good ductility and high charge mobility through reducing the central symmetry of the conjugated backbone units. Adv. Mater. *35*, 2209896.
29. Mun, J., Ochiai, Y., Wang, W., Zheng, Y., Zheng, Y.Q., Wu, H.C., Matsuhisa, N., Higashihara, T., Tok, J.B.H., Yun, Y., and Bao, Z. (2021). A design strategy for high mobility stretchable polymer semiconductors. Nat. Commun. *12*, 3572.
30. Wan, Q., Seo, S., Lee, S.W., Lee, J., Jeon, H., Kim, T.S., Kim, B.J., and Thompson, B.C. (2023). High-performance intrinsically stretchable polymer solar cell with record efficiency and stretchability enabled by thymine-functionalized terpolymer. J. Am. Chem. Soc. *145*, 11914–11920.
31. Chen, J., Zhu, M., Shao, M., Shi, W., Yang, J., Kuang, J., Wang, C., Gao, W., Zhu, C., Meng, R., et al. (2024). Molecular design of multifunctional integrated polymer semiconductors with intrinsic stretchability, high mobility, and intense luminescence. Adv. Mater. *36*, 2305987.
32. Yi, Z., Jiang, Y., Xu, L., Zhong, C., Yang, J., Wang, Q., Xiao, J., Liao, X., Wang, S., Guo, Y., et al. (2018). Triple acceptors in a polymeric architecture for balanced ambipolar transistors and high-gain inverters. Adv. Mater. *30*, 1801951.
33. Dang, D., Yu, D., and Wang, E. (2019). Conjugated donor–acceptor terpolymers toward high-efficiency polymer solar cells. Adv. Mater. *31*, 1807019.
34. Kang, T.E., Kim, K.-H., and Kim, B.J. (2014). Design of terpolymers as electron donors for highly efficient polymer solar cells. J. Mater. Chem. A Mater. *2*, 15252–15267.
35. Jung, S., Cho, Y., Ji, Y., Oh, J., Park, G., Kim, W., Jeong, S., Lee, S.M., Chen, S., Zhang, Y., and Yang, C. (2023). High-level periodic conjugated terpolymers through AA/BB monomer pair-type terpolymerization improve performance of polymer solar cells. Nano Energy *106*, 108059.
36. Ren, S., Ding, Y., Zhang, W., Wang, Z., Wang, S., and Yi, Z. (2023). Rational design of novel conjugated terpolymers based on diketopyrrolopyrrole and their applications to organic thin-film transistors. Polymers *15*, 3803.
37. Wang, Z., Wu, Y., Zhou, Q., Yang, L., Yi, Z., Yan, Y., Liu, Y., and Zhao, Y. (2023). Aggregation structure and glass transition of intrinsically stretchable semiconducting polymers. Matter *6*, 3434–3448.

38. Zhou, Q., Wang, Z., Yan, Y., Yang, L., Chi, K., Wu, Y., Li, W., Yi, Z., Liu, Y., and Zhao, Y. (2023). Strain-enhanced electrical performance in stretchable semiconducting polymers. npj Flex. Electron. *7*, 35.

39. O'Connor, B., Kline, R.J., Conrad, B.R., Richter, L.J., Gundlach, D., Toney, M.F., and DeLongchamp, D.M. (2011). Anisotropic structure and charge transport in highly strain-aligned regioregular poly(3-hexylthiophene). Adv. Funct. Mater. *21*, 3697–3705.

40. Kronemeijer, A.J., Gili, E., Shahid, M., Rivnay, J., Salleo, A., Heeney, M., and Sirringhaus, H. (2012). A selenophene-based low-bandgap donor–acceptor polymer leading to fast ambipolar logic. Adv. Mater. *24*, 1558–1565.

41. Lin, H.-W., Lee, W.-Y., and Chen, W.-C. (2012). Selenophene-DPP donor–acceptor conjugated polymer for high performance ambipolar field effect transistor and nonvolatile memory applications. J. Mater. Chem. *22*, 2120–2128.

42. Fan, B., Lin, F., Wu, X., Zhu, Z., and Jen, A.K.-Y. (2021). Selenium-containing organic photovoltaic materials. Acc. Chem. Res. *54*, 3906–3916.

43. Fu, B., Wang, C.Y., Rose, B.D., Jiang, Y., Chang, M., Chu, P.H., Yuan, Z., Fuentes-Hernandez, C., Kippelen, B., Brédas, J.L., et al. (2015). Molecular engineering of nonhalogenated solution-processable bithiazole-based electron-transport polymeric semiconductors. Chem. Mater. *27*, 2928–2937.

44. Teshima, Y., Yamanaka, K., Sato, Y., Ohkita, H., Mikie, T., Saito, M., and Osaka, I. (2024). Simple π-conjugated polymers based on bithiazole for nonfullerene organic photovoltaics. ACS Appl. Mater. Interfaces *16*, 3735–3743.

45. Rühle, V., Lukyanov, A., May, F., Schrader, M., Vehoff, T., Kirkpatrick, J., Baumeier, B., and Andrienko, D. (2011). Microscopic simulations of charge transport in disordered organic semiconductors. J. Chem. Theory Comput. *7*, 3335–3345.

46. Weigend, F., Häser, M., Patzelt, H., and Ahlrichs, R. (1998). RI-MP2: optimized auxiliary basis sets and demonstration of efficiency. Chem. Phys. Lett. *294*, 143–152.

47. Adamo, C., and Barone, V. (1999). Toward reliable density functional methods without adjustable parameters: The PBE0 model. J. Chem. Phys. *110*, 6158–6170.

48. Neese, F. (2012). The ORCA program system. WIREs Comput. Mol. Sci. *2*, 73–78.

49. Sarkar, T., Schneider, S.A., Ankonina, G., Hendsbee, A.D., Li, Y., Toney, M.F., and Frey, G.L. (2020). Tuning intra and intermolecular interactions for balanced hole and electron transport in semiconducting polymers. Chem. Mater. *32*, 7338–7346.

50. Chiu, M.-Y., Jeng, U., Su, C., Liang, K.S., and Wei, K. (2008). Simultaneous use of small-and wide-angle X-ray techniques to analyze nanometerscale phase separation in polymer heterojunction solar cells. Adv. Mater. *20*, 2573–2578.

51. Zheng, Y., Zhang, S., Tok, J.B.-H., and Bao, Z. (2022). Molecular design of stretchable polymer semiconductors: current progress and future directions. J. Am. Chem. Soc. *144*, 4699–4715.

52. Yashiro, K., Ito, T., and Tomita, Y. (2003). Molecular dynamics simulation of deformation behavior in amorphous polymer: nucleation of chain entanglements and network structure under uniaxial tension. Int. J. Mech. Sci. *45*, 1863–1876.

53. Kar, S., Cuddigan, J.L., and Greenfield, M.L. (2023). Simulating stress–strain behavior by using individual chains: Uniaxial deformation of amorphous cis-and trans-1, 4-polybutadiene. Polymers *15*, 1441.

54. Schrickx, H.M., Sen, P., Balar, N., and O'Connor, B.T. (2024). Strain alignment of conjugated polymers: Method, microstructure, and applications. Cell Rep. Phys. Sci. *5*, 102076.

55. Guo, C., Quinn, J., Sun, B., and Li, Y. (2016). Dramatically different charge transport properties of bisthienyl diketopyrrolopyrrole-bithiazole copolymers synthesized via two direct (hetero) arylation polymerization routes. Polym. Chem. *7*, 4515–4524.

56. Baumeier, B., Kirkpatrick, J., and Andrienko, D. (2010). Density-functional based determination of intermolecular charge transfer properties for large-scale morphologies. Phys. Chem. Chem. Phys. *12*, 11103–11113.